Available online at www.sciencedirect.com
ScienceDirect
International Journal of Heat and Mass Transfer 50 (2007) 4678–4687
International Journal of HEAT and MASS TRANSFER
www.elsevier.com/locate/ijhmt

Studies on piston and soret effects in a binary mixture supercritical fluid

A. Nakano *

National Institute of Advanced Industrial Science and Technology, 1-2-1 Namiki, Tsukuba East, Tsukuba, Ibaraki 305-8564, Japan

Received 23 May 2006; received in revised form 10 November 2006
Available online 3 May 2007

Abstract

Heat and mass transport phenomena in a binary mixture compressible supercritical fluid around the pseudo-critical line were investigated theoretically and numerically. In this study, we focused on supercritical artificial air with a composition of 79% nitrogen and 21% oxygen, and investigated the piston effect, the soret effect, and the interactions between these effects. We derived thermo-fluid dynamic equations, in which the compressibility of the fluid, the temperature, the pressure, and the concentration dependences of the entropy were taken into account. The governing equations were solved numerically by using the finite difference method. We could verify that the thermal energy was propagated by the piston effect in a binary mixture supercritical fluid, and the concentration change certainly occurred due to the soret effect. Moreover, we could also estimate the thermal diffusion ratio, which made a direct correlation between the temperature gradient and the concentration gradient.

Keywords: Piston effect; Soret effect; Artificial air

1. Introduction

The combination of very high thermal compressibility and small thermal diffusion around the pseudo-critical lines of fluids affects thermal energy propagation, leading to the formation of weak acoustic wave as carriers of thermal energy. Nowadays, this heat transport phenomenon is known as the piston effect. This effect was first detected in the microgravity experiment for measuring the specific heat of SF_6 near the critical point [1]. In the experiment, unexpected fast dynamic temperature propagation was observed. Straub et al. [2] verified the fast dynamic temperature propagation in a Spacelab Mission. Onuki et al. [3] provided an explanation about the fast heat transfer with adiabatic temperature propagation. Around the same time, Boukari et al. [4] analyzed this phenomenon from a thermodynamic point of view. Behringer et al. [5] investigated the adiabatic heating process in a pure fluid and a binary mixture. Zappoli et al. [6] accounted for the temperature propagation by solving the hydrodynamic equations and named the phenomenon "piston effect". Ferrel and Hao [7] and Zappoli et al. [8,9] investigated the effect, theoretically and numerically. In terms of past numerical endeavors, Zappoli et al. [10] successfully achieved the first direct numerical simulation of the piston effect in a single fluid. Frohlich et al. [11], Zhong et al. [12], Wilkinson et al. [13], and Garrabos et al. [14] carried out experiments on the piston effect and compared them with their theoretical predictions. Maekawa and Ishii [15] analyzed the piston effect from both macroscopic and microscopic points of view. Maekawa et al. [16], Shiroishi et al. [17], Furukawa and Onuki [18], and EL-Khouri and Carles [19] investigated the convective instabilities and discussed the interactions between the piston effect and convection. We also successfully observed the piston effect in supercritical nitrogen by using a laser holography interferometer [20,21] and confirmed the piston effect experimentally and numerically [22] around the pseudo-critical line. Recently, the piston

* Tel.: +81 29 861 7250; fax: +81 29 851 7523.
E-mail address: a.nakano@aist.go.jp

0017-9310/$ - see front matter © 2007 Elsevier Ltd. All rights reserved.
doi:10.1016/j.ijheatmasstransfer.2007.03.014

Nomenclature

C_p	specific heat at constant pressure, J/(mol K)
C_v	specific heat at constant volume, J/(mol K)
c	concentration
D	diffusion coefficient, m^2/s
D_T	thermal diffusion coefficient, m^2/s
k_T	thermal diffusion ratio (D_T/D)
M	molecular weight
P	pressure, Pa
Q	thermal energy flow per unit volume, J/m^3
s	entropy per unit mol, J/(mol K)
T	temperature, K
T_{MC}	Max–Condentherm temperature, K
t	time, s
u	velocity (x-direction), m/s
V	velocity, m/s
x	distance from the heat wall, m
$x^*(i)$	dimensionless computation domain ($i = 1, 2, \ldots, \max-1, \max$), where $x^*(1) = 0$ and $x^*(\max) = 1$

Greek symbols

ρ	density, mol/m^3
α	thermal diffusion factor
α_T	isothermal compressibility, 1/Pa
β	volume expansion coefficient, 1/K
γ	ratio of the specific heats, C_p/C_v
κ	thermal conductivity, W/(m K)
η	dynamic viscosity, Pa s
δ_{ik}	unit tensor
σ'_{ij}	viscous stress tensor
μ	chemical potential, J/mol

effect was successfully observed on acoustic time scales [23]. The piston effect has been mainly observed in a single-component fluid; however, the effect in a multi-component fluid has not been investigated thoroughly.

In our previous experiment, a critical opalescence phenomenon was observed near the critical point of air [24]. It meant that the molecules composing the air had coalesced into clusters. This implies that air possesses high compressibility and the piston effect can be observed in supercritical air. To confirm the validity of the supposition that the piston effect does occur, a laser holography interferometer was applied to visualize the piston effect in supercritical air [25]. However, its corroboration was insufficient, since air is composed of many substances. Then, we carried out a visualization experiment using artificial air composed of 79% nitrogen and 21% oxygen [26]. The spatial distribution of the density change due to heating was investigated and we successfully obtained typical density profiles due to the piston effect. Additionally, we also observed the density gradient in the bulk of fluid. It is formed by the soret effect. The soret effect is a phenomenon in which the temperature gradient induces a concentration flux. However, we have little evidence to support this effect. Then, we studied heat and mass transport mechanism in a supercritical binary mixture, theoretically and numerically. In this paper, we describe the theoretical consideration and the results of the numerical simulation for the supercritical artificial air around the pseudo-critical line.

2. Theoretical consideration

The following thermo-fluid equations were used to investigate the heat and mass transport mechanism in a binary mixture supercritical fluid [27]:

$$\frac{\partial \rho}{\partial t} + \frac{\partial(\rho V_i)}{\partial x_i} = 0, \tag{1}$$

$$\frac{\partial(\rho c)}{\partial t} + \frac{\partial(\rho c V_i)}{\partial x_i} = \frac{\partial}{\partial x_i}\left[\rho D\left(\frac{\partial c}{\partial x_i} + \frac{k_T}{T}\frac{\partial T}{\partial x_i}\right)\right], \tag{2}$$

$$\rho\frac{\partial V_i}{\partial t} + \rho V_j\frac{\partial V_i}{\partial x_j} = -\frac{\partial P}{\partial x_i} + \frac{\partial}{\partial x_j}\left[\eta\left(\frac{\partial V_i}{\partial x_j} + \frac{\partial V_j}{\partial x_i} - \frac{2}{3}\delta_{ik}\frac{\partial V_k}{\partial x_k}\right)\right], \tag{3}$$

$$\frac{dQ}{dt} = \sigma'_{ij}\frac{\partial V_i}{\partial x_j} - \frac{\partial}{\partial x_i}(q - \mu i), \tag{4}$$

where

$$q = \left[k_T\left(\frac{\partial \mu}{\partial c}\right)_{P,T} - T\left(\frac{\partial \mu}{\partial T}\right)_{P,c} + \mu\right] i - \kappa\frac{\partial T}{\partial x_i} \tag{5}$$

and

$$i = -\rho D\left[\frac{\partial c}{\partial x_i} + \frac{k_T}{T}\frac{\partial T}{\partial x_i}\right]. \tag{6}$$

Eqs. (1), (2), (3) and (4) represent the equation of continuity, the equation of concentration, the momentum equation of viscous fluid, and the energy balance equation, respectively. The suffixes i, j, k take the values 1, 2, 3 corresponding to the components of vectors and tensors along the axes x, y, z. In this study, the following assumptions were adopted that no significant pressure gradient was formed in the system due to heating, that there was no macroscopic motion in fluids, and that the second order small terms were ignored. The effect of gravity was not taken into account, here.

The pressure, P, in Eq. (3) was calculated from the following pressure derivative that

$$\frac{dP}{dt} = \frac{1}{\rho\alpha_T}\left[\frac{d\rho}{dt} - \left(\frac{\partial \rho}{\partial c}\right)_{P,T}\frac{dc}{dt}\right] + \frac{\beta}{\alpha_T}\frac{dT}{dt}. \tag{7}$$

For details, refer to the appendix.

On the other hand, the left term in Eq. (4), dQ/dt, can be expressed as $\rho T \cdot ds/dt$. Here, we take into account the temperature, the pressure, and the concentration dependences of the entropy. dQ/dt can be written as follows:

$$\frac{dQ}{dt} = \rho T \left\{ \left(\frac{\partial s}{\partial T}\right)_{P,c} \frac{dT}{dt} + \left(\frac{\partial s}{\partial P}\right)_{T,c} \frac{dP}{dt} + \left(\frac{\partial s}{\partial c}\right)_{P,T} \frac{dc}{dt} \right\}. \quad (8)$$

From a Maxwell relation and thermodynamic relations, we can obtain the following relations:

$$T\left(\frac{\partial s}{\partial P}\right)_{T,c} = -(C_P - C_v) \cdot \frac{\alpha_T}{\beta}, \quad (9)$$

$$T\left(\frac{\partial s}{\partial T}\right)_{P,c} = C_P, \quad (10)$$

and

$$\left(\frac{\partial s}{\partial c}\right)_{P,T} = -\left(\frac{\partial \mu}{\partial T}\right)_{P,c}. \quad (11)$$

Substituting Eqs. (7) and (9)–(11) into Eq. (8), dQ/dt can be written as follows:

$$\frac{dQ}{dt} = \rho C_v \frac{dT}{dt} - \frac{(C_P - C_v)}{\beta} \frac{\partial \rho}{dt} + \frac{(C_P - C_v)}{\beta} \left(\frac{\partial \rho}{\partial c}\right)_{P,T} \frac{\partial c}{dt} - \rho T \left(\frac{\partial \mu}{\partial T}\right)_{P,c} \frac{dc}{dt}. \quad (12)$$

On the other hand, the first term on the right-hand side of Eq. (4) can be written as

$$\sigma'_{ij} \frac{\partial V_i}{\partial x_j} \equiv \frac{1}{2}\eta \left(\frac{\partial V_i}{\partial x_j} + \frac{\partial V_j}{\partial x_i} - \frac{2}{3}\delta_{ik}\frac{\partial V_k}{\partial x_k}\right)^2. \quad (13)$$

Here, we ignored the effect of volumetric (bulk) viscosity [28–30]. If we discuss the heat and mass transport phenomena in the vicinity of the critical point of fluids ($T - T_c < 100$ m K: T_c is the critical temperature), we may need to take into account the effect of the volumetric viscosity [31,32]. But, in this study, we considered the phenomena around the pseudo-critical line. The system temperature and the pressure were relatively far from the critical point.

Substituting Eqs. (5), (6), (12) and (13) into Eq. (4), and using Eq. (2), the heat balance equation becomes the following:

$$\frac{d}{dt}\left[T - \left\{\frac{k_T}{C_v}\left(\frac{\partial \mu}{\partial c}\right)_{P,T} - \frac{(\gamma-1)}{\beta\rho}\left(\frac{\partial \rho}{\partial c}\right)_{P,T}\right\} c\right] + \left[1 - \frac{c}{\rho}\left(\frac{\partial \rho}{\partial c}\right)_{P,T}\right] \frac{(\gamma-1)}{\rho\beta} \frac{\partial(\rho V_i)}{\partial x_i} - \frac{V_i}{C_v}\left[k_T\left(\frac{\partial \mu}{\partial c}\right)_{P,T} - T\left(\frac{\partial \mu}{\partial T}\right)_{P,c}\right] \frac{\partial c}{\partial x_i} = \frac{1}{\rho C_v}\left[\frac{\partial}{\partial x_i}\left(\kappa \frac{\partial T}{\partial x_i}\right) + \frac{1}{2}\eta\left(\frac{\partial V_i}{\partial x_j} + \frac{\partial V_j}{\partial x_i} - \frac{2}{3}\delta_{ik}\frac{\partial V_k}{\partial x_k}\right)^2\right]. \quad (14)$$

For details, refer to the appendix. The governing equations were, therefore, Eqs. (1), (2), (3), (7), and (14). The independent variables were ρ, T, P, V_i, and c, respectively.

3. Calculation model

We assumed a one-dimensional model consisting of a very narrow, 0.01 m long tube of supercritical artificial air with the composition of 79% nitrogen and 21% oxygen. In this case, the Max–Condentherm (MC) temperature and the MC pressure are 131.558 K and 3.65314 MPa, respectively [33]. Unfortunately, we cannot show the exact values of the critical temperature and the critical pressure at this time. The critical point of a binary mixture can be only obtained with an experiment. As far as I know, there is no information about the critical point of the artificial air. But it could be predicted that the critical temperature and the critical pressure of the artificial air were slightly lower than the MC temperature and the MC pressure.

Fig. 1 shows the calculation model. The initial temperature, T_0, and the initial pressure, P_0, were 135 K and 4.35 MPa that were relatively higher than the MC temperature and the MC pressure. Heat was applied in step function from the left side. The temperature of the heated wall was suddenly increased by 100 m K in the first step. The opposite side wall kept the initial temperature. The governing equations for the one-dimensional model are shown as follows:

$$\frac{\partial \rho}{\partial t} + \frac{\partial(\rho u)}{\partial x} = 0, \quad (15)$$

$$\frac{\partial(\rho c)}{\partial t} + \frac{\partial(\rho c u)}{\partial x} - D\left(\frac{\partial c}{\partial x} + \frac{k_T}{T}\frac{\partial T}{\partial x}\right)\frac{\partial \rho}{\partial x} - \rho D\left(\frac{\partial^2 c}{\partial x^2} + \frac{k_T}{T}\frac{\partial^2 T}{\partial x^2}\right) = 0, \quad (16)$$

$$\frac{\partial(\rho u)}{\partial t} + \frac{\partial(\rho u^2 + P)}{\partial x} - \frac{4}{3}\eta\frac{\partial^2 u}{\partial x^2} = 0, \quad (17)$$

$$\frac{d}{dt}\left[T - \left\{\frac{k_T}{C_v}\left(\frac{\partial \mu}{\partial c}\right)_{P,T} - \frac{(\gamma-1)}{\beta\rho}\left(\frac{\partial \rho}{\partial c}\right)_{P,T}\right\} c\right] + \left[1 - \frac{c}{\rho}\left(\frac{\partial \rho}{\partial c}\right)_{P,T}\right] \frac{(\gamma-1)}{\rho\beta}\frac{\partial(\rho u)}{\partial x} - \frac{u}{C_v}\left[k_T\left(\frac{\partial \mu}{\partial c}\right)_{P,T} - T\left(\frac{\partial \mu}{\partial T}\right)_{P,c}\right]\frac{\partial c}{\partial x} - \frac{8}{9}\frac{\eta}{\rho C_v}\left(\frac{\partial u}{\partial x}\right)^2 - \frac{\kappa}{\rho C_v}\frac{\partial^2 T}{\partial x^2} = 0, \quad (18)$$

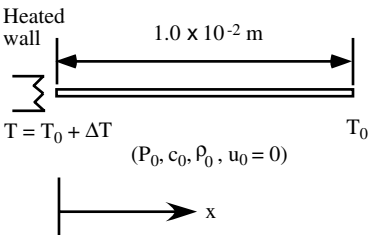

Fig. 1. One-dimensional calculation model.

Table 1
Thermo-physical properties

T (K)	P (MPa)	ρ (mol/m^3)	C_v (J/mol K)	C_P (J/mol K)	γ [C_P/C_v]	α_T (1/Pa) 10^{-6}	β (1/K)	η (μPa s)	κ (W/m K)	$\left(\frac{\partial\rho}{\partial c}\right)_{P,T}$ (mol/m^3)	$\left(\frac{\partial\mu}{\partial c}\right)_{P,T}$ (J/mol)	$\left(\frac{\partial\mu}{\partial T}\right)_{P,c}$ (J/mol K)
135.0	4.35	13036.8	29.5615	444.720	15.044	0.9628	0.1963	20.7817	0.0574	52050	−2258.5	−125.6765

$$\frac{dP}{dt} = \frac{1}{\rho\alpha_T}\left[\frac{d\rho}{dt} - \left(\frac{\partial\rho}{\partial c}\right)_{P,T}\frac{dc}{dt}\right] + \frac{\beta}{\alpha_T}\frac{dT}{dt}. \tag{19}$$

In this analysis, we assumed small temperature variation and small concentration change. Then, we gave the constant values to the induced variables, C_v, γ, α_T, β, η, κ, $\left(\frac{\partial\rho}{\partial c}\right)_{P,T}$, $\left(\frac{\partial\mu}{\partial c}\right)_{P,T}$, and $\left(\frac{\partial\mu}{\partial T}\right)_{P,c}$. Table 1 shows the thermo-physical properties, which correspond to the value under the conditions of T_0 and P_0, with the composition of 79% nitrogen and 21% oxygen. They were obtained from the database software [33]. As for the concentration, c, we monitored the concentration of oxygen.

To solve the governing equations, we had two unknown factors that were the diffusion coefficient, D, and the thermal diffusion ratio, k_T. As for D, we estimated the value, 5×10^{-8} m^2/s by using the following equation, which was proposed by Mathur and Thodos [34]:

$$D \cdot B \cdot \rho_R = 10.7 \times 10^{-5} \cdot T_R, \tag{20}$$

where $B = M^{1/2}P_c^{1/3}/T_c^{5/6}$. ρ_R and T_R are the reduced density, ρ/ρ_c, and the reduced temperature, T/T_c, respectively. The subscript, c, stands for the critical point. This equation is not proposed for a binary mixture fluid, but it is acceptable to obtain an approximate value for D [35].

On the other hand, there was no information concerning k_T for the nitrogen–oxygen system near the critical point. Waldmann [36] reported the thermal diffusion factor, α, of nitrogen–oxygen system. The α is expressed as the k_T divided by the relative concentrations of each component, that is essentially the same with the k_T. The values of α are <0.0011, 0.012, and 0.017 when the temperatures are 89 K, 194 K, and 372 K, respectively. However, these data were obtained with a pressure lower than the atmospheric pressure. To examine the sign and the order of the k_T under the conditions of 135 K and 4.35 MPa, we calculated it by using Chapman's first order approximation with the Lennard-Jones potential [37]. Under the conditions, the k_T was assigned the negative and the estimated value was −0.000612, which was extremely small value. On the other hand, Rutherford and Roof [38] measured the thermal diffusion factor, α, in methane-*n*-butane system in the critical region. The data suggest that the value of α becomes large as the system approaches the critical point. We considered that the estimated value of k_T could not used near the critical point.

As for the thermal diffusion, Onuki [39] introduced the dynamic crossover in nearly azeotropic fluid mixture. In case of ^{3}He–^{4}He mixture, the sign of k_T shows negative and the absolute value of k_T goes up exponentially as the system temperature approaches the critical temperature [40,41]. The nitrogen–oxygen mixture can be regarded as the nearly azeotropic fluid mixture because the critical points of nitrogen and oxygen are relatively close. Then, we adopted negative k_T, and selected the following three values that $k_T = -0.5, -1.0$ and -2.0 in this numerical analysis. The thermal diffusion ratio, k_T, indicates the ratio between the thermal diffusion coefficient, D_T, and the diffusion coefficient, D. We investigated the cases that the absolute values of D_T were a half, an equal, and two times as large as the D. To seek an appropriate value for k_T was also one of the important objectives of this study.

Here, dimensionless governing equations were deduced from the governing equations and those were solved by the explicit Mac–Cormack method with the FCT algorithm. At the computational domain boundaries, $x^*(1)$ and $x^*(\max)$, we gave that $T_{x^*(1)} = 135.1\ \mathrm{K}/T_{MC}$, $T_{x^*(\max)} = 135.0\ \mathrm{K}/T_{MC}$, $P_{x^*(1)} = P_{x^*(2)}$, $P_{x^*(\max)} = P_{x^*(\max-1)}$, $\rho_{x^*(1)} = \rho_{x^*(2)}$, $\rho_{x^*(\max)} = \rho_{x^*(\max-1)}$, and $u_{x^*(1)} = u_{x^*(\max)} = 0$. The c at the boundaries was obtained from ρc which was calculated from Eq. (16) by using the independent variables in the previous time-step at $x^*(1)$, $x^*(2)$, $x^*(\max - 1)$, and $x^*(\max)$.

4. Results and discussion

Numerical calculations were successfully performed without any numerical instability when we assigned a certain negative value to k_T. This means that oxygen, which is a high-boiling component, moves toward the heated wall. We will show the calculation results on short and long time scales.

Fig. 2 shows the calculation results on short time scales in the case of $k_T = -0.5$. Fig. 2a shows the pressure distributions at every 20 μs. It can be seen that a pressure wave propagates into the bulk of fluid and repeats the reflection. Fig. 2b shows the temperature distributions. Temperature wave also propagates as the pressure wave and the system temperature rise quickly. It is noted from these figures that the thermal energy propagates with the velocity of sound. This suggests that the thermal energy is propagated by the piston effect. The piston effect is initiated by the high compressibility of artificial air around the pseudo-critical line. A thin diffusive thermal boundary layer, which is formed at the heated wall–fluid interface, expands due to the high compressibility. This expansion acts as a piston, generating an acoustic wave. Thermal conversion of this

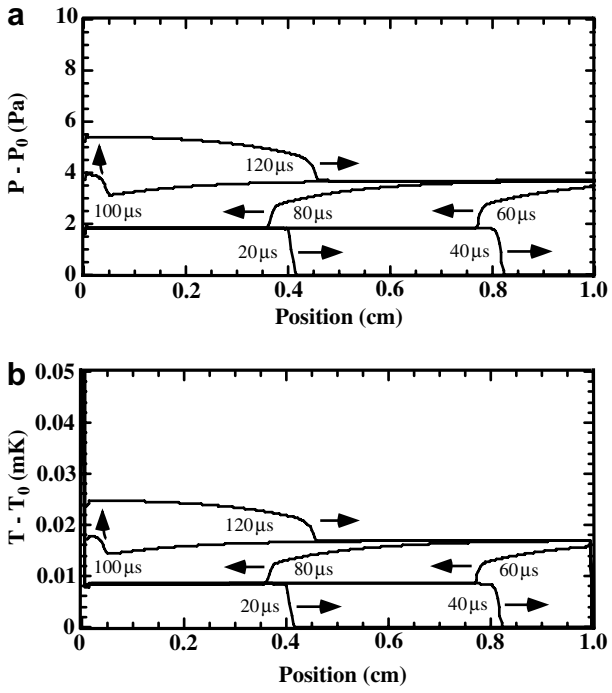

Fig. 2. Calculation results on short time scales ($k_T = -0.5$): (a) pressure distributions and (b) temperature distributions.

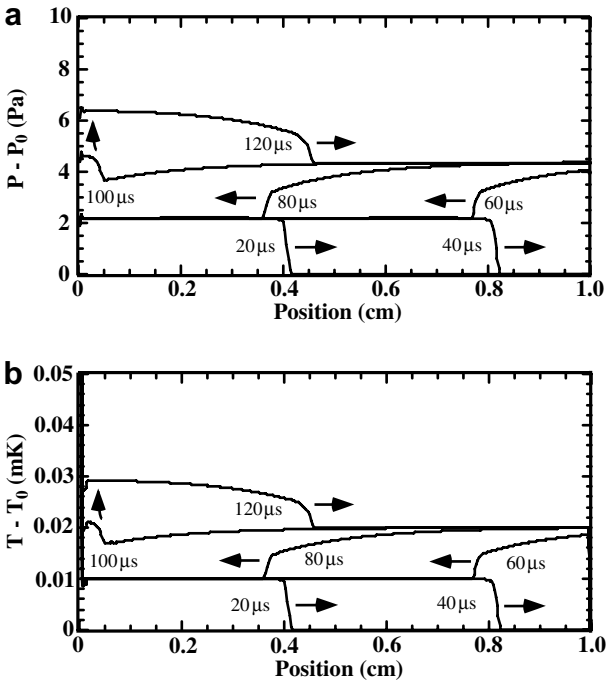

Fig. 3. Calculation results on short time scales ($k_T = -1.0$): (a) pressure distributions and (b) temperature distributions.

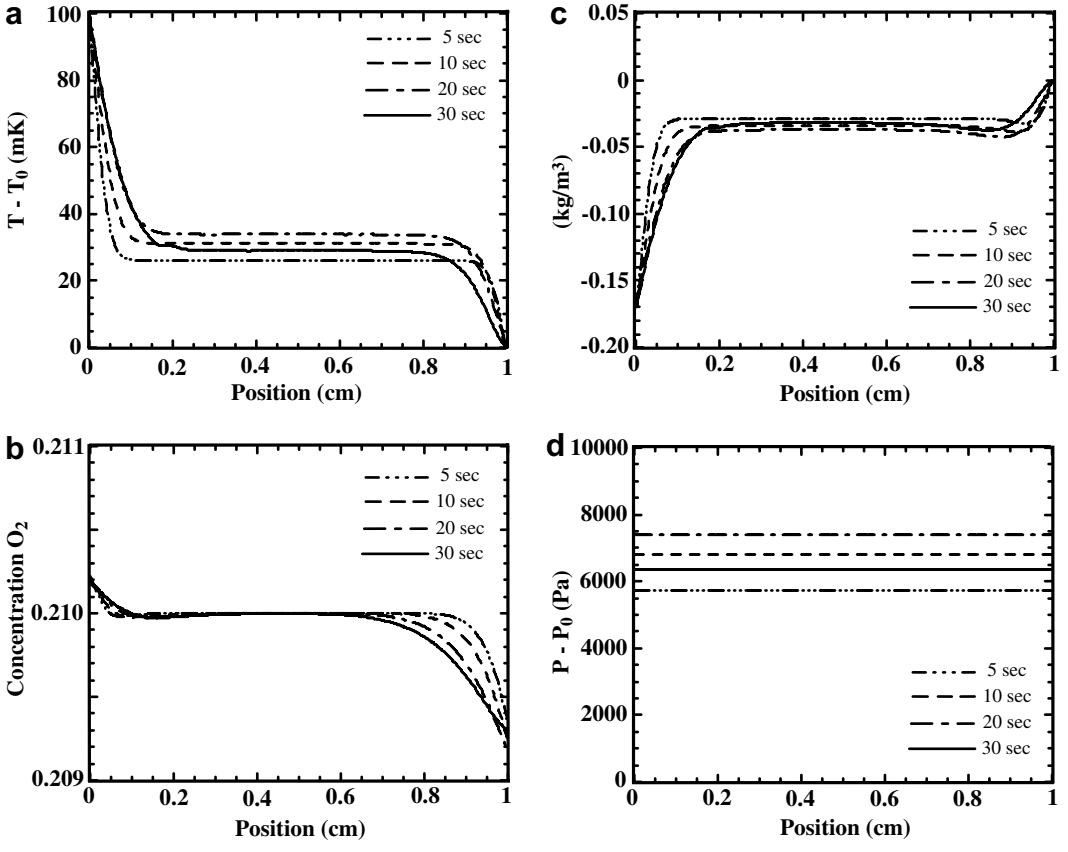

Fig. 4. Calculation results on long time scales ($k_T = -0.5$): (a) temperature distributions, (b) concentration distributions of oxygen, (c) spatial distributions of the density variation and (d) pressure distributions.

pressure wave can heat the fluid in an adiabatic manner. As for the concentration, we could not observe any concentration change in the time range.

Fig. 3 shows the calculation results in the case of $k_T = -1.0$. Fig. 3a and b shows the pressure distributions and the temperature distributions, respectively. These figures also suggest that temperature wave propagates as the pressure wave, and the temperature wave propagates with the velocity of sound. It is noted that the magnitudes of the pressure and temperature waves are slightly larger than those of the previous case. We also could not see any concentration change in the time range same as before.

From these calculation results on short time scales, it could be confirmed that the thermal energy was propagated by the piston effect, even in the case of the binary mixture supercritical fluid. However, we could not see any concentration changes on the time scales because the piston effect was driven by propagation, whereas the soret effect was driven by diffusion. Then, we carried out the calculations on long time scales to investigate the soret effect and the interactions between the piston effect and the soret effect.

Fig. 4 shows the calculation results on long time scales in the case of $k_T = -0.5$. The temperature distributions at $\Delta t = 5$, 10, 20, and 30 s are shown in Fig. 4a, where Δt shows the elapsed time after the onset of heating. It can be seen in each temperature distribution that a homogeneous temperature field appears in the bulk of the fluid and that the steep thermal boundary layers form near both walls. The temperature distributions show the typical temperature profile due to the piston effect. It is noted that the level of the constant temperature field becomes small after $\Delta t = 20$ s, and that the gradients of the thermal boundary layer on both sides become small. Fig. 4b shows the concentration distributions of oxygen. It is noted that the concentration of oxygen at the heated wall rises, and that the concentration lowers in the opposite side. Fig. 4c shows the results of the spatial distributions of the density variation, $\Delta\rho$. In this case, the density variation on the right-side wall had been adjusted to correspond to the origin of the y-axis. The density distributions show the shapes that inverted the temperature distributions shown in Fig. 4a upside down. This suggests that the density variation with temperature change was dominant. The effect of concentration upon the density was not so large. Fig. 4d shows the pressure distributions. We note that the pressure increases until $\Delta t = 20$ s, but that the pressure slightly goes down after that. It seems that it has not reached the steady state in 30 s.

Fig. 5 shows the calculation results in the case of $k_T = -1.0$. Fig. 5a shows the temperature distributions. The temperature varied like in the previous case. The level of the constant temperature field increased until $\Delta t = 20$ s,

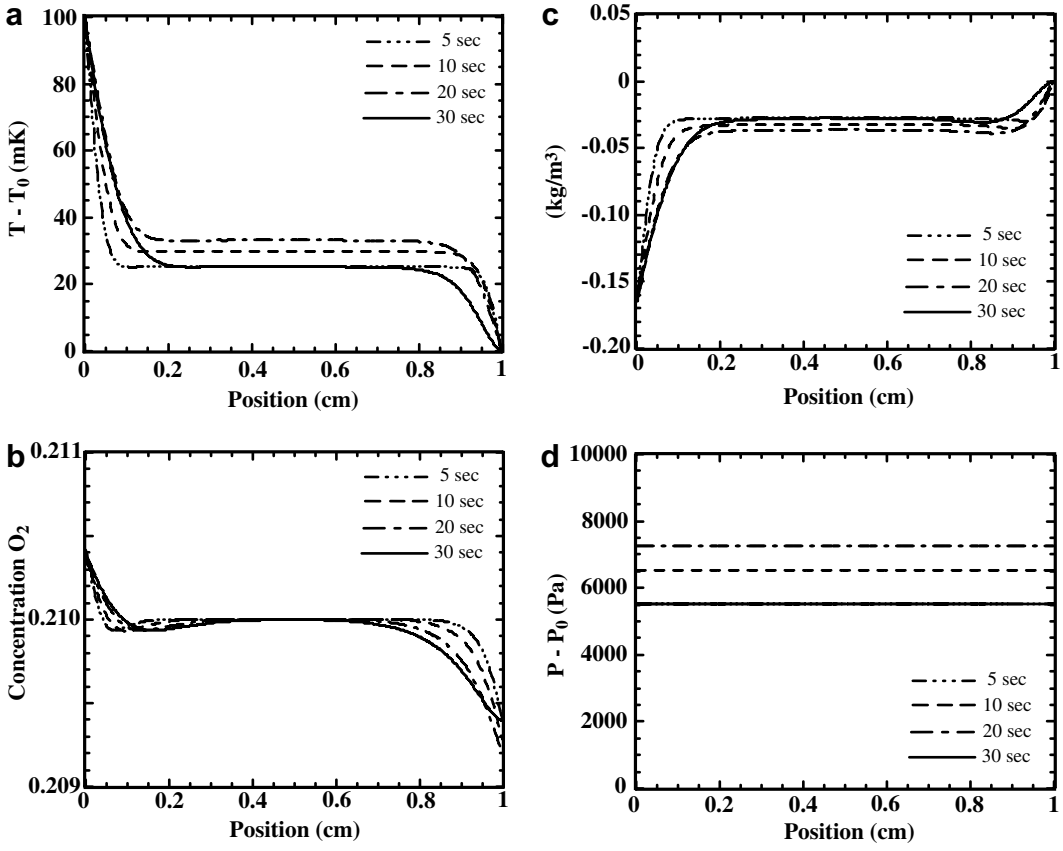

Fig. 5. Calculation results on long time scales ($k_T = -1.0$): (a) temperature distributions, (b) concentration distributions of oxygen, (c) spatial distributions of the density variation and (d) pressure distributions. The line at 30 s overlaps with the line at 5 s.

but after that, the temperature went down. The decrement of the temperature was larger than in the previous case. It is noted from Fig. 5b that the concentration of oxygen at the heated wall is increased as compared with the results

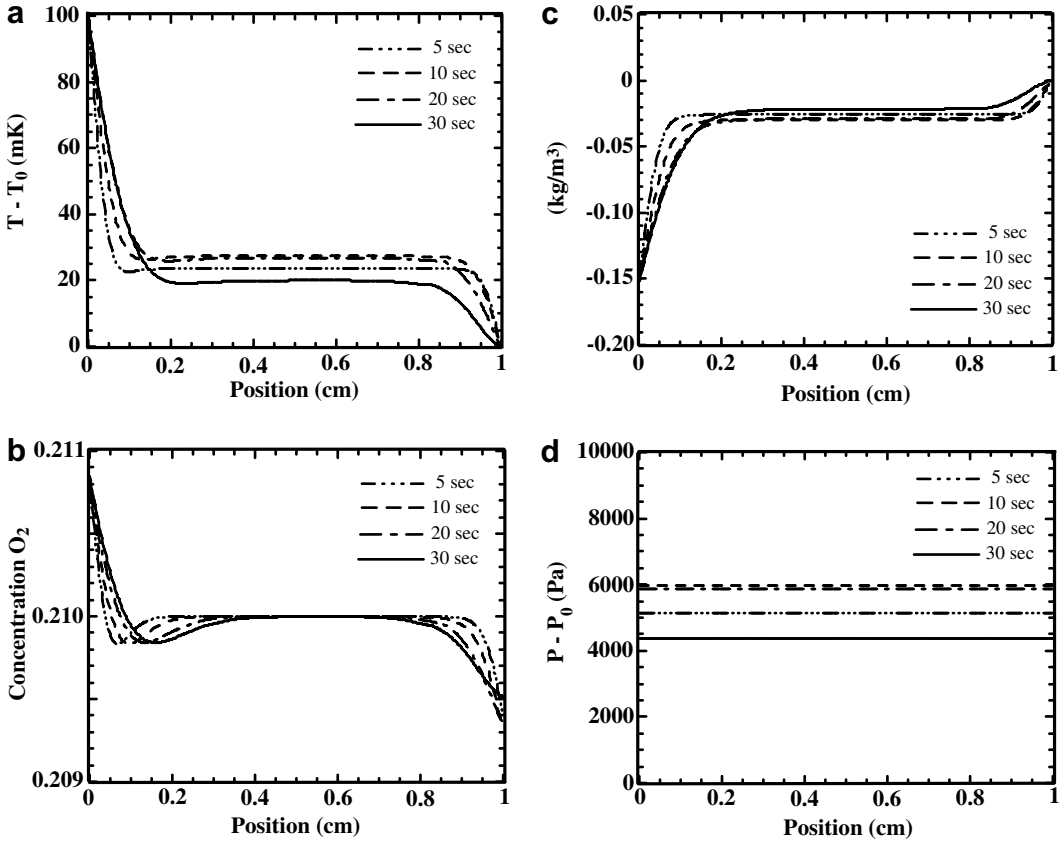

Fig. 6. Calculation results on long time scales ($k_T = -2.0$): (a) temperature distributions, (b) concentration distributions of oxygen, (c) spatial distributions of the density variation and (d) pressure distributions.

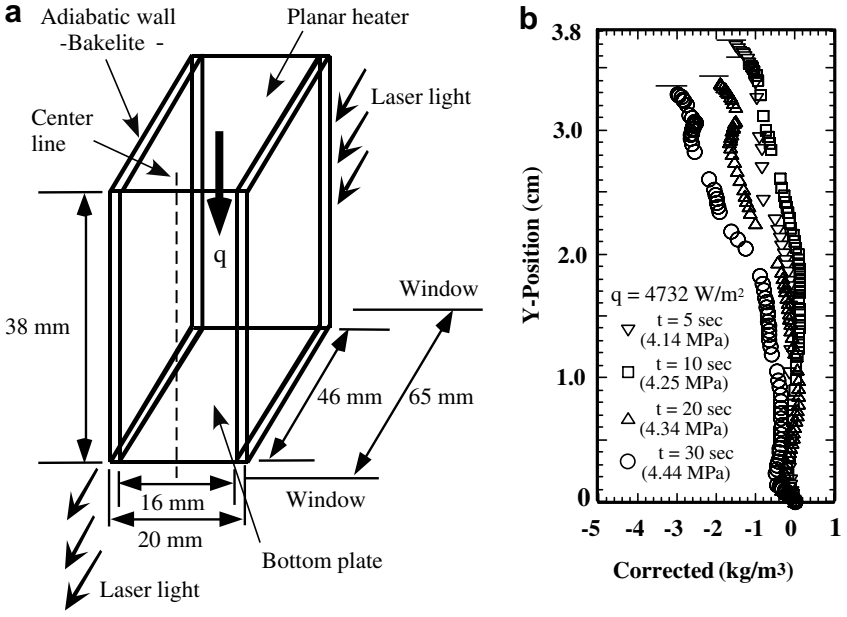

Fig. 7. Introduction of the experimental results in Ref. [26]: (a) schematic illustration of the experimental cell and (b) spatial distributions of corrected $\Delta\rho$ when heat was added from the top.

shown in Fig. 4b. Fig. 5c shows the spatial distributions of $\Delta\rho$. Fundamentally, the density profiles are the same as in the case of $k_T = -0.5$. Fig. 5d shows the pressure distributions. It is also noted that the pressure increases until $\Delta t = 20$ s, but that the pressure drops to the level at $\Delta t = 5$ s when $\Delta t = 30$ s.

Fig. 6 shows the calculation results in the case of $k_T = -2.0$. We can also observe the typical temperature profiles due to the piston effect in each temperature distribution shown in Fig. 6a, but the temperature at the bulk of the fluid is suppressed as compared with the previous two cases where $k_T = -0.5$ and -1.0. It is noted from Fig. 6b that the concentration of oxygen at the heated wall side is about twice as large as compared with the case of $k_T = -1.0$. It seems that the concentration change is proportional to the absolute value of k_T. Fig. 6c shows the spatial distributions of $\Delta\rho$. The density variation was also suppressed because the density mainly varied with temperature change. It is noted that a gentle density gradient can be seen in the bulk of fluid in the result of $\Delta t = 30$ s. This seems to be consistent with the experimental results obtained from our previous study. Fig. 7 shows a part of the experimental results published in Ref. [26]. Fig. 7a shows the schematic of the experimental cell. Heat was added from the top of the cell. Fig. 7b shows the spatial distribution of the corrected $\Delta\rho$ on the centerline of the cell. It is noted that relatively large density gradient can be observed in the bulk of fluid. For details, refer to Ref. [26]. Fig. 6d shows the pressure distributions. After $\Delta t = 10$ s, the pressure gradually decreases. As the absolute value of k_T increases, the decrements of the temperature and the pressure increase.

We could successfully simulate the heat and mass transport phenomena in supercritical artificial air. However, at this moment, it is difficult to compare the calculation results with the experimental results. Because, if the comparison be made, a calculation should be needed where the temperature raise at the heated wall is about 5 K. In such a case, the values of the thermo-physical properties largely change. It is difficult to obtain a reliable solution by using the present numerical code. We need to prepare the data table of the thermo-physical properties for different temperatures, different pressures, and different mole fractions. Furthermore, it is desirable to obtain experimental data of the diffusion coefficient, D, and the thermal diffusion ratio, k_T.

5. Conclusion

We successfully simulated the heat and mass transport phenomena in supercritical artificial air that was a binary mixture supercritical fluid with the composition of 79% nitrogen and 21% oxygen. We could verify the existence of the piston effect in the supercritical artificial air. It was found that the piston effect was the dominant heat transport mechanism in the initial stage, and the concentration change due to the soret effect appeared several seconds after. From this study, we could determine the sign of the thermal diffusion ratio, k_T. The sign of k_T was negative near the critical point. Further, the k_T took the value over -2 under the condition of 135 K and 4.35 MPa. However, to determine the certain value of k_T, we have to carry out an experiment for the concentration measurement.

Acknowledgement

The author wishes to give special thanks to Dr. M. Shiraishi, Prof. M. Shoji from Kanagawa Univ., Prof. M. Murakami from Univ. of Tsukuba, for useful suggestions. The author acknowledges a lot of discussions on the numerical simulation with Dr. T. Munakata. Prof. A. Onuki from Kyoto Univ., Prof. Y. Miura from Nagoya Univ., Emeritus Prof. T. Sato from Tohoku Univ., Dr. M. Ohnishi from JAXA, Dr. S. Yoshihara from JAXA, and Dr. S. Adachi from JAXA are also thanked for their fruitful advice.

Appendix

- About the pressure derivative dP/dt.
  The density derivative can be written as follows:

$$\frac{d\rho}{dt} = \left(\frac{\partial\rho}{\partial T}\right)_{P,c}\frac{dT}{dt} + \left(\frac{\partial\rho}{\partial P}\right)_{T,c}\frac{dP}{dt} + \left(\frac{\partial\rho}{\partial c}\right)_{P,T}\frac{dc}{dt}. \tag{A.1}$$

  Substituting the following relations, $\left(\frac{d\rho}{\partial T}\right)_{P,c} = -\rho\beta$, and $\left(\frac{\partial\rho}{\partial P}\right)_{T,c} = \rho\alpha_T$, which were obtained from the van der Waal's equation, into Eq. (A.1), we have

$$\frac{dP}{dt} = \frac{1}{\rho\alpha_T}\left[\frac{d\rho}{dt} - \left(\frac{\partial\rho}{\partial c}\right)_{P,T}\frac{dc}{dt}\right] + \frac{\beta}{\alpha_T}\frac{dT}{dt}. \tag{A.2}$$

- About the energy balance equation.
  From Eq. (4), the energy balance equation can be written as follows:

$$\frac{dQ}{dt} + \mathrm{div}(q - \mu i) = \sigma'_{ij}\frac{\partial V_i}{\partial x_j}. \tag{A.3}$$

  Substituting Eqs. (5), (6) and (12) into Eq. (A.3), the left-hand side can be written as follows:

$$\begin{aligned}
&\frac{dQ}{dt} + \mathrm{div}(q - \mu i)\\
&\quad = \rho C_v\frac{dT}{dt} + \frac{(C_P - C_v)}{\beta}\mathrm{div}(\rho V)\\
&\qquad + \frac{(C_P - C_v)}{\beta}\left(\frac{\partial\rho}{\partial c}\right)_{P,T}\frac{\partial c}{dt} - \rho T\left(\frac{\partial\mu}{\partial T}\right)_{P,c}\frac{dc}{dt}\\
&\qquad + \mathrm{div}\left[\left\{k_T\left(\frac{\partial\mu}{\partial c}\right)_{P,T} - T\left(\frac{\partial\mu}{\partial T}\right)_{P,c}\right\}\right.\\
&\qquad \left.\cdot\left\{-\rho D\left(\mathrm{grad}\cdot c + \frac{k_T}{T}\mathrm{grad}\cdot T\right)\right\} - .\kappa\cdot\mathrm{grad}\cdot T\right],
\end{aligned} \tag{A.4}$$

where we used the equation of continuity to obtain the above equation. Next, we assume small temperature variation and small concentration change. In that case, $\left(\frac{\partial\rho}{\partial c}\right)_{P,T}$, $\left(\frac{\partial\mu}{\partial c}\right)_{P,T}$, and $\left(\frac{\partial\mu}{\partial T}\right)_{P,c}$ can be treated as the constant values. The right-hand side of Eq. (A.4) can be written as follows:

$$\begin{aligned}
&\rho C_v \frac{\mathrm{d}T}{\mathrm{d}t} + \frac{(C_P - C_v)}{\beta}\mathrm{div}(\rho V) + \frac{(C_P - C_v)}{\beta}\left(\frac{\partial \rho}{\partial c}\right)_{P,T}\frac{\partial c}{\mathrm{d}t} \\
&\quad - \rho T\left(\frac{\partial \mu}{\partial T}\right)_{P,c}\frac{\mathrm{d}c}{\mathrm{d}t} - \left[k_T\left(\frac{\partial \mu}{\partial c}\right)_{P,T} - T\left(\frac{\partial \mu}{\partial T}\right)_{P,c}\right] \\
&\quad \cdot \mathrm{div}\left[\rho D\left(\mathrm{grad}\cdot c + \frac{k_T}{T}\mathrm{grad}\cdot T\right)\right] - \mathrm{div}[\kappa \cdot \mathrm{grad}\cdot T] \\
&= \rho C_v \frac{\mathrm{d}T}{\mathrm{d}t} + \frac{(C_P - C_v)}{\beta}\mathrm{div}(\rho V) \\
&\quad + \frac{(C_P - C_v)}{\beta}\left(\frac{\partial \rho}{\partial c}\right)_{P,T}\frac{\partial c}{\mathrm{d}t} - \rho T\left(\frac{\partial \mu}{\partial T}\right)_{P,c}\frac{\mathrm{d}c}{\mathrm{d}t} \\
&\quad - \left[k_T\left(\frac{\partial \mu}{\partial c}\right)_{P,T} - T\left(\frac{\partial \mu}{\partial T}\right)_{P,c}\right]\cdot\left[\rho\frac{\partial c}{\partial t} + \rho V\cdot\mathrm{grad}\cdot c\right] \\
&\quad - \mathrm{div}[\kappa\cdot\mathrm{grad}\cdot T] \\
&= \rho C_v \frac{\mathrm{d}T}{\mathrm{d}t} + \left[\frac{(C_P - C_v)}{\beta}\left(\frac{\partial \rho}{\partial c}\right)_{P,T} - \rho k_T\left(\frac{\partial \mu}{\partial c}\right)_{P,T}\right]\cdot\frac{\partial c}{\mathrm{d}t} \\
&\quad + \frac{(C_P - C_v)}{\beta}\mathrm{div}(\rho V) - \rho V\left[k_T\left(\frac{\partial \mu}{\partial c}\right)_{P,T} - T\left(\frac{\partial \mu}{\partial T}\right)_{P,c}\right]\cdot\mathrm{grad}\cdot c \\
&\quad - \mathrm{div}[\kappa\cdot\mathrm{grad}\cdot T]. \qquad (A.5)
\end{aligned}$$

Using the above expression, the energy balance equation can be written as follows:

$$\begin{aligned}
&\rho C_v \frac{\mathrm{d}T}{\mathrm{d}t} + \left[\frac{(C_P - C_v)}{\beta}\left(\frac{\partial \rho}{\partial c}\right)_{P,T} - \rho k_T\left(\frac{\partial \mu}{\partial c}\right)_{P,T}\right]\cdot\frac{\partial c}{\mathrm{d}t} \\
&\quad + \frac{(C_P - C_v)}{\beta}\mathrm{div}(\rho V) - \rho V\left[k_T\left(\frac{\partial \mu}{\partial c}\right)_{P,T} - T\left(\frac{\partial \mu}{\partial T}\right)_{P,c}\right]\cdot\mathrm{grad}\cdot c \\
&= \mathrm{div}[\kappa\cdot\mathrm{grad}T] + \sigma'_{ij}\frac{\partial V_i}{\partial x_j}. \qquad (A.6)
\end{aligned}$$

Dividing the both sides by ρC_v, one obtains

$$\begin{aligned}
&\frac{\mathrm{d}T}{\mathrm{d}t} - \frac{k_T}{C_v}\left(\frac{\partial \mu}{\partial c}\right)_{P,T}\frac{\mathrm{d}c}{\mathrm{d}t} + \frac{(\gamma-1)}{\rho\beta}\left(\frac{\partial \rho}{\partial c}\right)_{P,T}\frac{\mathrm{d}c}{\mathrm{d}t} \\
&\quad + \frac{(\gamma-1)}{\rho\beta}\mathrm{div}(\rho V) - \frac{V}{C_v}\left[k_T\left(\frac{\partial \mu}{\partial c}\right)_{P,T} - T\left(\frac{\partial \mu}{\partial T}\right)_{P,c}\right]\mathrm{grad}\cdot c \\
&= \frac{1}{\rho C_v}\left[\mathrm{div}\{\kappa\cdot\mathrm{grad}\cdot T\} + \sigma'_{ij}\frac{\partial V_i}{\partial x_j}\right]. \qquad (A.7)
\end{aligned}$$

Here, the 3rd term in the left-hand side can be written as

$$\begin{aligned}
&\frac{(\gamma-1)}{\rho\beta}\left(\frac{\partial \rho}{\partial c}\right)_{P,T}\frac{\mathrm{d}c}{\mathrm{d}t} \\
&= \frac{(\gamma-1)}{\beta}\left(\frac{\partial \rho}{\partial c}\right)_{P,T}\left[\frac{\mathrm{d}}{\mathrm{d}t}\left(\frac{c}{\rho}\right) - c\frac{\mathrm{d}}{\mathrm{d}t}\left(\frac{1}{\rho}\right)\right] \\
&= \frac{(\gamma-1)}{\beta}\left(\frac{\partial \rho}{\partial c}\right)_{P,T}\frac{\mathrm{d}}{\mathrm{d}t}\left(\frac{c}{\rho}\right) - \frac{(\gamma-1)c}{\rho^2\beta}\left(\frac{\partial \rho}{\partial c}\right)_{P,T}\mathrm{div}(\rho V). \qquad (A.8)
\end{aligned}$$

Substituting Eq. (A.8) into Eq. (A.7), the final equation can be obtained as follows:

$$\begin{aligned}
&\frac{\mathrm{d}}{\mathrm{d}t}\left[T - \left\{\frac{k_T}{C_v}\left(\frac{\partial \mu}{\partial c}\right)_{P,T} - \frac{(\gamma-1)}{\rho\beta}\left(\frac{\partial \rho}{\partial c}\right)_{P,T}\right\}c\right] \\
&\quad + \left[1 - \frac{c}{\rho}\left(\frac{\partial \rho}{\partial c}\right)_{P,T}\right]\frac{(\gamma-1)}{\rho\beta}\mathrm{div}(\rho V) \\
&\quad - \frac{V}{C_v}\left[k_T\left(\frac{\partial \mu}{\partial c}\right)_{P,T} - T\left(\frac{\partial \mu}{\partial T}\right)_{P,c}\right]\mathrm{grad}\cdot c \\
&= \frac{1}{\rho C_v}\left[\mathrm{div}\{\kappa\cdot\mathrm{grad}\cdot T\} + \sigma'_{ij}\frac{\partial V_i}{\partial x_j}\right]. \qquad (A.9)
\end{aligned}$$

References

[1] K. Nitsche, J. Straub, The critical "HUMP" of C_v under microgravity results from D1-Spacelab experiment "WARMEKAPAZITAT", in: Proc. 6th European Symposium on Material Science Under Microgravity Conditions SP-256 1986, pp. 109–116.

[2] J. Straub, L. Eicher, A. Haupt, Dynamic temperature propagation in a fluid near its critical point observed under microgravity during the German spacelab mission D-2, Phys. Rev. E 51 (1995) 5556–5563.

[3] A. Onuki, H. Hao, R.A. Ferrell, Fast adiabatic equilibration in a single-component fluid near the liquid–vapor critical point, Phys. Rev. A 41 (1990) 2256–2259.

[4] H. Boukari, J.N. Shaumeyer, M.E. Briggs, R.W. Gammon, Critical speeding up in pure fluids, Phys. Rev. A 41 (1990) 2260–2263.

[5] R.P. Behringer, A. Onuki, H. Meyer, Thermal equilibration of fluids near the liquid–vapor critical point: ^{3}He and ^{3}He–^{4}He mixtures, J. Low Temp. Phys. 81 (1990) 71–102.

[6] B. Zappoli, D. Bailly, Y. Garrabos, B. LeNeindre, P. Guenoun, D. Beysens, Anomalous heat transport by the piston effect in supercritical fluids under zero gravity, Phys. Rev. A 41 (1990) 2264–2267.

[7] R.A. Ferrell, H. Hao, Adiabatic temperature changes in a one-component fluid near the liquid–vapor critical point, Physica A 197 (1993) 23–46.

[8] B. Zappoli, A. Durand-Daubin, Heat and mass transport in a near supercritical fluid, Phys. Fluids 6 (1994) 1929–1936.

[9] B. Zappoli, P. Carles, The thermo-acoustic nature of the critical speeding up, Eur. J. Mech. B/Fluids 14 (1995) 41–65.

[10] B. Zappoli, S. Amiroudine, P. Carles, J. Ouazzani, Thermoacoustic and buoyancy-driven transport in a square side-heat cavity filled with a near-critical fluid, J. Fluid Mech. 316 (1996) 53–72.

[11] T. Frohlich, P. Guenoun, M. Bonetti, F. Perrot, D. Beysens, Y. Garrabos, B. Le Neindre, P. Bravais, Adiabatic versus conductive heat transfer in off-critical SF_6 in the absence of convection, Phys. Rev. E 54 (1996) 1544–1549.

[12] F. Zhong, A. Kogan, H. Meyer, Thermal response of a fluid near its critical point: ^{3}He at $T > T_c$, J. Low Temp. Phys. 108 (1997) 161–189.

[13] R.A. Wilkinson, G.A. Zimmerli, H. Hao, M.R. Moldover, R.F. Berg, W.L. Johnson, R.A. Ferrell, R.W. Gammon, Equilibration near the liquid–vapor critical point in microgravity, Phys. Rev. E 57 (1998) 436–448.

[14] Y. Garrabos, M. Bonetti, D. Beysens, F. Perrot, T. Frohlich, P. Carles, B. Zappoli, Relaxation of a supercritical fluid after a heat pulse in the absence of gravity effects: Theory and experiments, Phys. Rev. E 57 (1998) 5665–5681.

[15] T. Maekawa, K. Ishii, Temperature propagation in a single component critical fluid, Thermal Sci. Eng. 5 (1997) 15–23.

[16] T. Maekawa, K. Ishii, M. Ohnishi, S. Yoshihara, Convective instabilities induced in a critical fluid, Adv. Space Res. 29 (2002) 589–598.

[17] Y. Shiroishi, T. Maekawa, K. Ishii, H. Azuma, S. Yoshihara, M. Ohnishi, Convective instabilities induced in a critical fluid, The 6th ASME–JSME Thermal Engineering Joint Conf. (2003) TED-AJ03-576.

[18] A. Furukawa, A. Onuki, Convective heat transport in compressible fluids, Phys. Rev. E 66 (2002) 016302 1–016302 14.
[19] L. EL-Khouri, P. Carles, Thermoacoustic and buoyancy-driven convection in supercritical fluids, in: Proc. 12th Int. Heat Transfer Conf., vol. 2, 2002, pp. 531–536.
[20] A. Nakano, M. Shirashi, M. Murakami, Application of laser holography interferometer to heat transport phenomena near the critical point of nitrogen, Cryogenics 41 (2001) 429–435.
[21] A. Nakano, M. Shiraishi, Piston effect in supercritical nitrogen around the pseudo-critical line, Int. Commun. Heat Mass Transfer 32 (2005) 1152–1164.
[22] A. Nakano, M. Shirashi, Numerical simulation for the piston effect and thermal diffusion observed in supercritical nitrogen, Cryogenics 44 (2004) 867–873.
[23] Y. Miura, S. Yoshihara, M. Ohnishi, K. Honda, M. Matsumoto, J. Kawai, M. Ishikawa, H. Kobayashi, A. Onuki, High-speed observation of the piston effect near the gas–liquid critical point, Phys. Rev. E 74 (2006) 010101 1–010101 4.
[24] A. Nakano, M. Shiraishi, Visualization study of heat transfer phenomenon in supercritical air near the Max–Condentherm point, Cryog. Eng. 37 (2002) 265–270 (in Japanese).
[25] A. Nakano, M. Shiraishi, Investigation of heat and mass transport phenomena in supercritical air, Cryog. Eng. 38 (2003) 152–157 (in Japanese).
[26] A. Nakano, M. Shirashi, Visualization for heat and mass transport phenomena in supercritical artificial air, Cryogenics 45 (2005) 557–565.
[27] L.D. Landau, E.M. Lifshitz, Fluid Mechanics, Pergamon Press, London, 1959.
[28] A. Onuki, Dynamic equations and bulk viscosity near the gas–liquid critical point, Phys. Rev. E 55 (1997) 403–420.
[29] P. Carles, The effect of bulk viscosity on temperature relaxation near the critical point, Phys. Fluids 10 (1998) 2164–2176.
[30] K.A. Gills, I. Shinder, M.R. Moldover, Bulk viscosity thermoacoustic boundary layers and adsorption near the critical point of xenon, Phys. Rev. Lett. 97 (2006) 104502 1–104502 4.
[31] P. Carles, K. Dadzie, Two typical time scales of the piston effect, Phys. Rev. E 71 (2005) 066310 1–066310 13.
[32] M. Ishikawa, Y. Miura, M. Ohnishi, S. Yoshihara, M. Sakurai, H. Kobayashi, K. Honda, M. Matsumoto, J. Kawai, Piston dynamics of CO_2 fluid near critical point, Bull. Eur. Low Gravity Res. Assoc. 24 (2005) 135–136.
[33] NIST Database 72 "NIST-AIRPROPS Ver. 1.0".
[34] G.P. Mathur, G. Thodos, The self-diffusivity of substances in the gaseous and liquid states, AIChE J. 11 (1965) 613–616.
[35] R.C. Reid, J.M. Pravsnitz, T.K. Sherwood, The Properties of Gases and Liquids, McGraw-Hill Inc., 1977.
[36] V.L. Waldmann, Uber die Druck- und Temperaturabhangigkeit der Warmeerscheinungen bei der Diffusion, Z. Naturforsch. 4a (1949) 105–117 (in Germany).
[37] J.O. Hirschfelder, C.F. Curtiss, R.B. Bird, Molecular Theory of Gases and Liquids, John Wiley & Sons Inc., New York, London, Sydney, 1964.
[38] W.M. Rutherford, J.G. Roof, Thermal diffusion in methane-*n*-butane mixtures in the critical region, J. Phys. Chem. 63 (1959) 1506–1511.
[39] A. Onuki, Phase Transition Dynamics, Cambridge Univ. Press, 2002.
[40] L.H. Cohen, M.L. Dingus, H. Meyer, Thermal diffusion measurements near the liquid–vapor critical point, Phys. Rev. Lett. 50 (1983) 1058–1061.
[41] H. Meyer, L.H. Cohen, Static and dynamic properties of helium near the liquid–vapor critical point: Comparison of experiments in mixtures with predictions, Phys. Rev. A 38 (1988) 2081–2088.